Individual Variations in Human Cone Photoreceptor Packing Density: Variations with Refractive Error

Toco Yuen Ping Chui, HongXin Song, and Stephen A. Burns

Purpose. To measure the variation in human cone photoreceptor packing density across the retina, both within an individual and between individuals with different refractive errors.

Methods. A high-resolution adaptive optics scanning laser ophthalmoscope was used to image the cones of 11 human eyes. Five subjects with emmetropia and six subjects with myopia were tested (+0.50 to −7.50 D). For each subject, four approximately 10° × 1.5° strips of cone images were obtained. Each strip started at the fovea and proceeded toward the periphery along the four primary meridians. The position of each cone within the sampling windows was digitized manually by the investigator. From these cone counts, the density of the cones was calculated for a set of fixed distances from the fovea at locations throughout the image.

Results. Cone photoreceptor packing density decreased from 27,712 cells/mm^2 to 7,070 cells/mm^2 from a retinal eccentricity of 0.30 to 3.40 mm along the superior meridian in five emmetropic eyes. Cone photoreceptor packing density (cells per square millimeter) was significantly lower in myopic eyes than in emmetropic eyes. At a given location, there was considerable individual variation in cone photoreceptor packing density, although more than 20% of the variance could be accounted for by differences in axial length.

Conclusions. The results provide a baseline analysis of individual difference in cone photoreceptor packing density in healthy human eyes. As predicted by retinal stretching models, cone photoreceptor packing density is lower in highly myopic eyes than in emmetropic eyes. (*Invest Ophthalmol Vis Sci.* 2008;49:4679–4687) DOI:10.1167/iovs.08-2135

Adaptive optics retinal imaging,[1–4] now allows routine imaging of retinal cone photoreceptors in the living human retina. This approach is now providing direct measurements of how cone photoreceptors are affected by diseases such as retinitis pigmentosa and cone–rod dystropy[5,6] as well as other conditions.[7] However, to make full use of these measurements in the study of disease, we must have a solid understanding of the variation in cone packing density in normal eyes. Currently, the histologic data of Curcio et al.[8] have been used as a normal control data set in most studies investigating in vivo cone photoreceptor packing. In their studies, they showed that there were individual variations in central cone packing density, but less in the near periphery, a result in agreement with other in vivo techniques.[9,10] In addition, she and collaborators have found some changes in cone numbers with aging.[11,12] Furthermore, the distribution of cones across the retina is uneven, with a slight tendency to show a higher density of cones along the horizontal meridian.[8]

While these changes have not been fully investigated in vivo, there is also likely to be sources of individual differences in cone packing density that do not arise from age or disease. One such cause is likely to be eye size. Although the cones reach their final number early in development, the eye continues to grow through adolescence and even into adulthood.[13–16] Thus, it is expected that if a constant number of cones are distributed across various size eyes, there could be large individual differences due to eye size. Since eye length varies from 22 to 28 mm in length, we could expect the surface area to vary by 60%. Although the details of eye growth are not quite so straightforward,[17–21] it is clear that in terms of the number of cones per square millimeter of the retina, we expect a significant dependence on eye length, an expectation that is supported by the finding of decreased cone spacing at 2° in the temporal retina in myopic eyes.[22] The dependence of cone density on eye length has also been indirectly implied in psychophysical studies of the effect of myopia on peripheral visual acuity. Axially myopic eyes are larger than emmetropic eyes because of the elongation of the vitreous chamber.[13–16] In the eyes of persons with axial myopia, there is reduced visual acuity and contrast sensitivity (Applegate RA, et al. *IOVS* 2001; 42:ARVO Abstract 2657).[18–21,23–27] These impairments in visual performance can be attributed to both reduced neural sampling density associated with retinal stretching[18,20,27] and reduced optical quality in persons with myopia.[28,29] In the present study, we examined individual differences in cone packing density across the retina in young adults. We also measured the variation in cone packing density across the retina both within an individual and between-individuals with different refractive errors and axial lengths.

Methods

Subjects

Eleven healthy subjects (five men and six women; age range 21–31 years, mean, 26.6) participated in these measurements. All subjects received a complete eye examination, including a subjective refraction and retinal imaging using a Heidelberg Retina Angiograph (HRA; Heidelberg Engineering GmbH, Heidelberg, Germany). Exclusion criteria for this study included any retinal disease or systemic diseases. Spherical equivalent refractive errors ranged from +0.50 to −7.50 D (mean −2.48, SD 2.82) with astigmatism less than −1.00 D when referenced to the spectacle plane. Subjects were classified into three groups based on their refractive error. Group 1 (five subjects) was emmetropic, with a range of spherical equivalent refractive error from +0.50 to 0.00 D (mean +0.15 D, SD 0.22). Group 2 (four subjects) consisted of persons with low-to-moderate myopia, with refractive errors ranging from −2.75 to −4.50 D (mean −3.63 D, SD 0.78). Group 3 (two subjects) was high myopic, with refractive errors ranging from −6.00 to −7.50 D (mean −6.75 D, SD 1.06). All subjects had best corrected visual acuity of 20/20 or better. The right eye of each subject was imaged in this experiment. All adaptive optics scanning laser ophthalmoscope (AOSLO) imaging sessions were conducted after the pupils were di-

From the School of Optometry, Indiana University, Bloomington, Indiana.

Supported by National Eye Institute Grants R01-EY14375 and R01-EY04395.

Submitted for publication April 7, 2008; revised May 19, 2008; accepted August 12, 2008.

Disclosure: **T.Y.P. Chui**, None; **H. Song**, None; **S.A. Burns**, None

The publication costs of this article were defrayed in part by page charge payment. This article must therefore be marked "*advertisement*" in accordance with 18 U.S.C. §1734 solely to indicate this fact.

Corresponding author: Stephen A. Burns, School of Optometry, Indiana University, 800 E. Atwater Avenue, Bloomington, IN 47405; staburns@indiana.edu.

lated with 0.5% tropicamide. The pupil diameter measured under room illumination was equal to or greater than 6 mm before starting the experiment. Informed consent was obtained after a full explanation of the procedures and consequences of the study. This study protocol was approved by Indiana University Institutional Review Board and complied with the requirements of the Declaration of Helsinki.

Axial Length Measurements

One drop of 0.5% proparacaine hydrochloride was instilled as a corneal surface anesthetic to facilitate the measurement of axial length by A-scan ultrasonography (A/B-scan; Advent; Mentor O&O, Norwell, MA). Axial length measurements were conducted after AOSLO imaging was completed. A mean of five axial length measurements were obtained for each subject. Axial length ranged from 22.80 to 27.47 mm (mean 24.45, SD 1.49). The mean axial length and SD were 23.24 ± 0.53, 24.72 ± 0.36, and 26.98 ± 0.70 mm in groups 1, 2, and 3, respectively.

Apparatus

The Indiana AOSLO system has been described in detail elsewhere.[30] In general, it is composed of three primary optical subsystems of importance in the present study: the wavefront sensor and deformable mirror subsystem, the confocal imaging subsystem, and the wide-field imaging subsystem. The light source for high-resolution imaging was provided by a super luminescent diode (SLD) that had a 50-nm bandwidth centered at 840 nm. The adaptive optics control of the system was maintained by using a deformable mirror (MEMS; Boston Micromachines, Cambridge, MA) and custom software. Wavefront errors were detected with a Shack-Hartmann sensor operating at 15 Hz. The imaging raster was provided by an 8-kHz horizontal scanning galvanometer and a programmable vertical scan galvanometer. For these experiments, the vertical scan was programmed to provide full frame images of 512 × 512 pixels at a frame rate of 15 Hz. Light returning from the retina passes through a confocal aperture optically conjugate to the retinal plane. For this study, the confocal aperture was either 12 or 24 μm relative to the retina, depending on which aperture produced the best image quality before the eyes were dilated. The subject's head movements were stabilized by using a wax impression of the mouth and a head rest. They were instructed to fixate an illuminated green LED. Fixation LEDs were arranged in an 8 × 8 array. For a given fixation position, a set of steering mirrors positioned the beam sequentially across the retina, with a range of 9° vertically and 10° horizontally.

Procedures

Images were collected as short sections of sequential video frames (30 frames). As soon as a region of retina was imaged, the steering mirrors were moved under the experimenter's control, so that an adjacent section of overlapping retina was imaged, and the next set of frames was collected. For each subject, we obtained four approximately 10° sets of cone images. Each set started at the fovea and proceeded toward the periphery along either the horizontal meridian (both nasal and temporal) or the vertical meridian (both superior and inferior). Typically, a single acquisition of 30 frames was sufficient to collect a data set suitable for cone quantification. To relate the separate video frames to each other, it was necessary to align them properly. Image montaging was performed offline by finding corresponding points between the selected images using cross correlation (MatLab; The MathWorks, Inc., Natick, MA). Each image in the montage was generated from a single frame without averaging. All montages locations were verified by comparison to the subject's HRA fundus images. A comparison of HRA and cone image strips is shown in Figures 1a and 1b.

Measuring the Cone Packing Density

A set of 150 × 150-pixel sampling windows at different retinal eccentricities were located on the montages (Fig. 1c). These sampling windows were chosen so that an apparently complete set of retinal cones was optically resolved. That is, none was obscured by blood vessels. The position of each cone within the sampling windows was then digitized manually by the investigator in the software by clicking a mouse on the cone and marking its location on the image, to ensure that no cone was counted twice and that none was excluded. From these cone counts, the density of cones was calculated for a set of fixed distances from the fovea for locations throughout the montage.

Computing the Retinal Magnification Factor

Differences in optical magnification and thus retinal image size, created by different axial lengths and different correction lenses cause the relation between pixel coordinates and retinal dimensions (expressed in millimeters), measured by an AOSLO, to vary. For a given visual angle, retinal dimensions (in millimeters) will be larger in a myopic retina than in an emmetropic retina, due to the longer axial length. This larger retinal dimension affects the calculation of cone packing density in cells per square millimeter. For this reason, we converted pixels to retinal position, by using the measured axial length for each eye and computing a retinal magnification factor (RMF) that converts from external angles to retinal dimensions based on the axial length of the individual eyes being imaged and the optics of the system. In our system, we corrected ametropia using both a built-in Badal optometer (which, because it is telecentric, does not alter the angular magnification with changes in defocus) and trial lenses (which in our system do change the angular magnification). When trial lenses were used, they

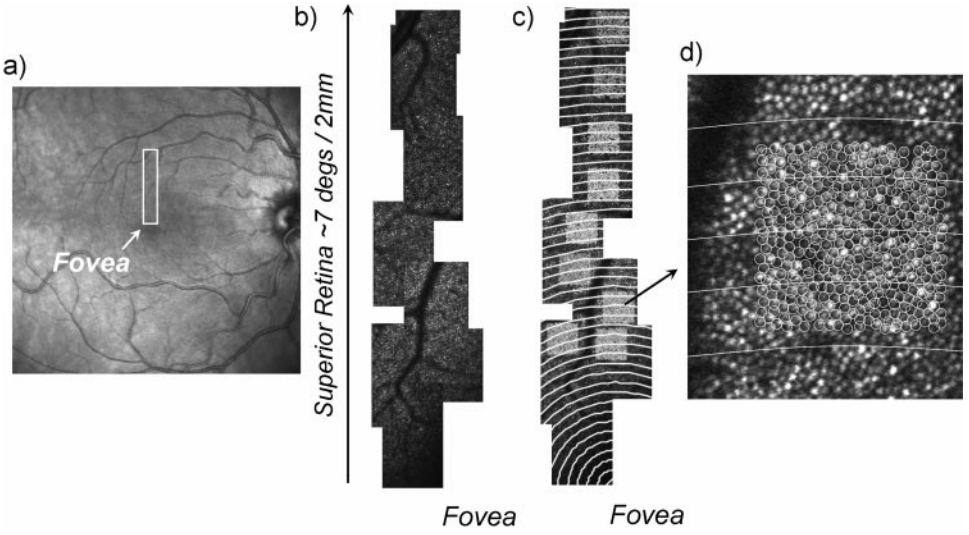

Figure 1. (**a**) HRA fundus image of subject 01. *Box*: the region for high-resolution imaging in the superior field. (**b**) Montage of a series of high-resolution images reaching from the fovea (*bottom right*) to the superior periphery. (**c**) Same region of the retina, indicating regions for cone counting, with constant distances from the fovea indicated by *concentric white circles*. (**d**) One of the regions of interest expanded to show individual cones as well as the distance bins.

were placed in the AOSLO system at 15 mm from the pupil plane. To correct for the effect of the trial lens, we used a standard reduced eye model to calculate the magnification factor. Individual RMF was computed (Zemax Development Corp., Bellevue, WA). The RMF was estimated for each eye based on the correction lenses added to the system and the subject's axial length. To double check the computed relative RMF, we compared the RMF computed from the software with the RMF calculated by the ratio of pixel distance between two cones of the same subject when wearing contact lenses and when using trial lenses. The test subject had a refractive error of −4.50 D and an axial length of 25.07 mm. We measured a 2% difference between the corrected intercone distances for the two imaging conditions when the images were corrected according to our model (Fig. 2). A similar calibration was performed on a model eye, where the axial length (the distance from the lens to a target) was varied, and the system was used to correct the induced defocus optically. Results were similar.

Results

Five subjects with emmetropia, four subjects with low-to-moderate myopia and two subjects with high myopia were tested. The relationship between spherical equivalent refractive error and axial length is shown in Figure 3. As expected, significant correlation was found between the axial length and refractive error ($r = -0.92$, $P < 0.0001$). As expected from the resolution of our system (2.8 μm for a diffraction limited emmetropic eye), we were unable to image the central foveal cones, but we were able to count cones from approximately 1° to 10°. Figure 4 shows a temporal montage of subject 10 (axial length, 23.71 mm) ranging from 0° retinal eccentricity to 10°. The squares indicate regions that are shown in high resolution in the bottom row.

Cone Packing Density in Emmetropic Eyes

Variation of cone packing density with retinal eccentricity along the superior meridian in five emmetropic subjects is shown in Figure 5. The *y*-axis in the graph indicates the cone packing density in 1000 cells/mm^2. According to our data, cone packing density decreased from 27,712 to 7,070 cells/mm^2 from the retinal eccentricity of 0.30 to 3.40 mm along the superior meridian. The dashed curve in Figure 5 is the result of a fit of a power law relation between retinal eccentricity and cone packing density. The solid curve is the mean cone packing density in seven human eyes from a previous anatomic study on human cone topography.[8] The power law fit of the cone packing density in all four meridians is shown with heavy solid curves in Figure 6. The cone packing density data for the emmetropic eyes are in reasonable agreement with the data reported by Curcio et al.[8] obtained in postmortem measurements.

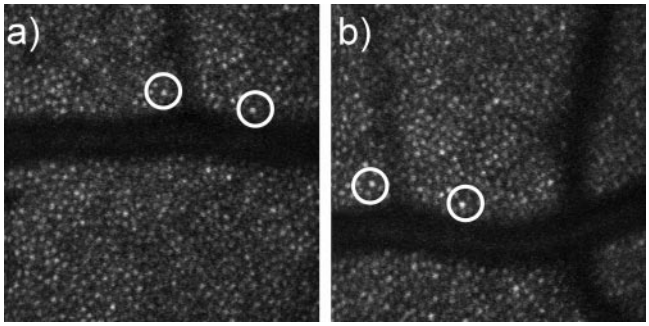

Figure 2. AOSLO images of a −4.50-D myope. Single-frame AOSLO images (**a**) with spectacle lens correction. (**b**) With contact lens correction. Pixel distance is determined by the distance between two distinctive cones (*circles*). When corrected using our optical model, the results were within 2% of each other, despite the relatively large magnification change due to the use of trial lenses in one of the conditions.

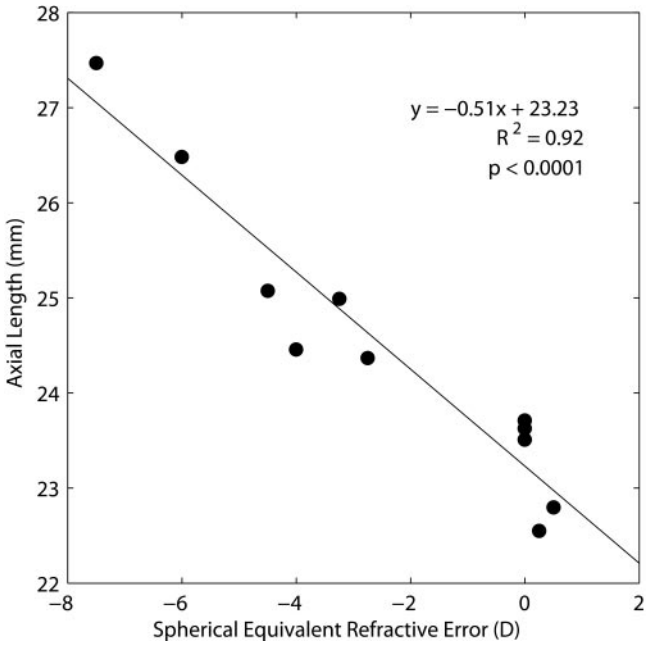

Figure 3. Relationship between axial length and spherical equivalent refractive error in subjects' right eyes. *Solid line*: linear regression to the data.

Variation of Cone Packing Density in Three Groups of Refractive Error

Figure 7 compares cone packing densities obtained from the three groups of subjects along four meridians. There was considerable variability among the six tested myopic subjects. As with the emmetropic subjects, a power law fit was used to estimate the overall trend of cone packing density change as a function of retinal eccentricity in each subject group. The results of these fits for the three subject groups are shown in Figure 6. Table 1 shows the mean cone packing density for each subject group in two retinal locations and along each of the four meridians. The retinal regions considered for this analysis were a region approximately 3° from the fovea and a region approximately 6° from the fovea (area 1 = 0.9–1.0 mm and area 2 = 1.8–2.0 mm retinal eccentricity). To avoid unintended biases due to the interaction of the steepness of the cone packing gradient and constraints on sampling locations imposed by blood vessels, we did not include regions closer to the fovea than 900 μm in the summary comparison. Cone packing density was higher in group 1 than in the other two groups in all meridians and retinal areas except for area 2 in the nasal meridian. For all groups the cone packing density was the lowest in the inferior meridian. To test the significance of the interactions between refractive error group, meridian, and eccentricity, a three-way ANOVA was performed (SPSS, ver. 15.0; SPSS, Chicago, IL). The ANOVA results are presented in Table 2. The significance of the mean differences was computed by performing two-way comparisons between groups at each of the retinal eccentricities. Table 3 presents the results for a pair-wise comparison of the means across areas 1 and 2, and shows that cone packing densities were significantly higher in refractive error group 1 than in refractive error groups 2 and 3.

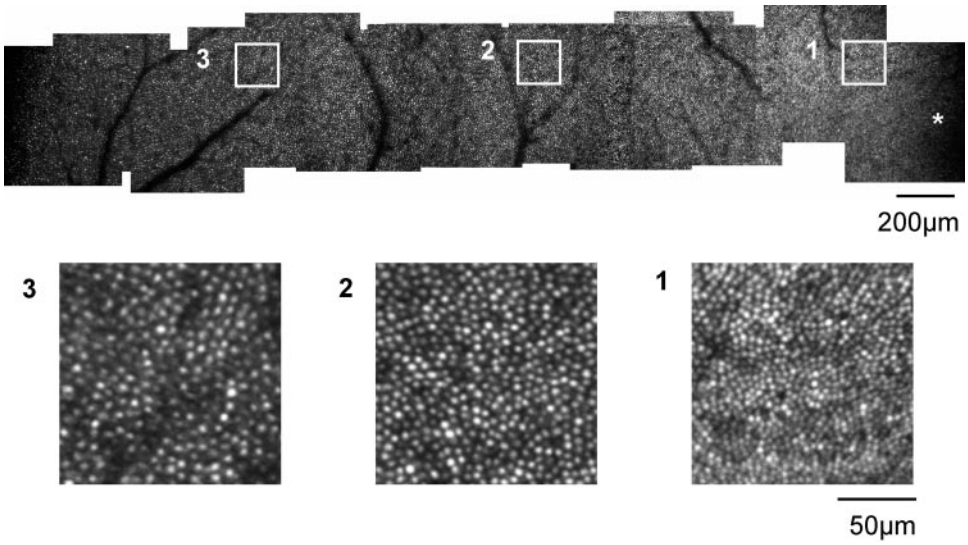

FIGURE 4. *Top*: temporal montage from subject 10, an emmetrope with an axial length of 23.71 mm. This montage spans approximately 10° from the fovea (⋆) to the temporal retina (*left*). *Bottom*: Averaged subregions matching the areas in the *squares* in the *top* panel. Cone photoreceptors are resolved at retinal locations from approximately 1° to 10°. Scale bar: (*top*) 200 μm; (*bottom*) 50 μm.

Variation of Cone Packing Density with Different Axial Lengths and Refractive Errors

Table 4 summarizes the regression slopes of estimated cone density in four meridians as a function of axial length and refractive error. Figure 8 presents the variation of cone packing density with axial lengths and refractive error. The estimated cone packing densities at the retinal eccentricity of 1, 1.5, and 2 mm were computed from the power law fits for each subject. Linear regressions between cone packing density estimates and axial length and refractive error are shown by the solid lines. All regression slopes are statistically significant ($P < 0.05$). Figure 9 shows that, in terms of the estimated cone packing densities expressed in angular units, there was little variation with axial length and refractive error at the retinal eccentricities of 3°, 5°, and 7°.

DISCUSSION

We used the AOSLO to make systematic measurements of cone packing density across the retina. In the present study, data were obtained from five subjects with emmetropia and six subjects with myopia. We found that in the emmetropic subjects the cone packing density expressed in cells per square millimeter was in overall agreement with the data reported by Curcio et al.[8] Other anatomic studies have found similar re-

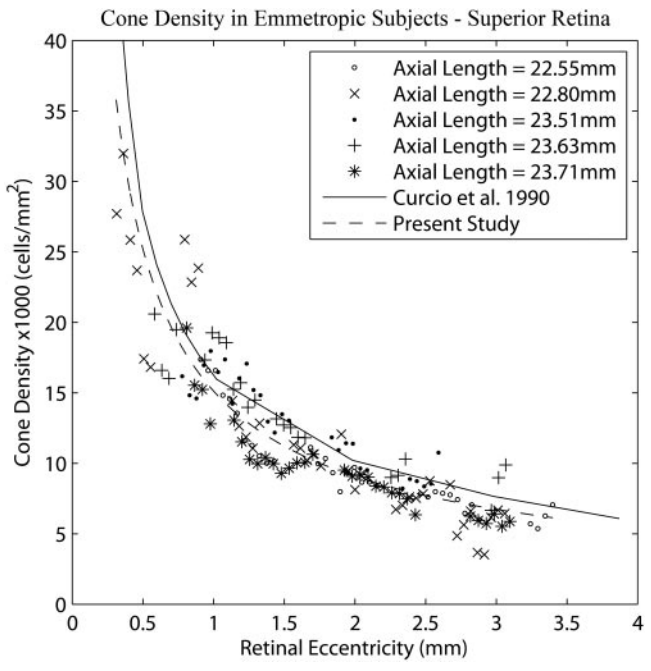

FIGURE 5. Variation of cone packing density with retinal eccentricity along the superior meridian in five emmetropic subjects. Cone packing density decreased from 27,712 to 7,070 cells/mm^2 from the retinal eccentricity of 0.30 to 3.40 mm along the superior meridian. *Solid curve*: result from Curcio et al.[8] *Dashed curve*: power law fit for the five subjects with emmetropia in group 1.

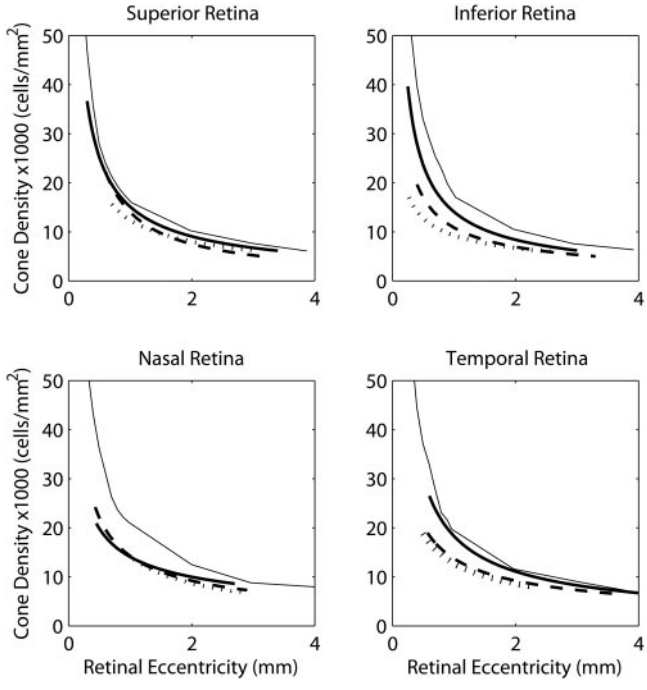

FIGURE 6. Comparisons of cone packing densities obtained from the study of Curcio et al.[8] (*solid curves*) and data from subjects with emmetropia (*heavy solid curves*), low-to-moderate myopia (*dashed curves*), and high myopia (*dotted curves*) in each of the four meridians in the present study. The data from the present study were fit using power law fitting, and the lines are based on this fitting.

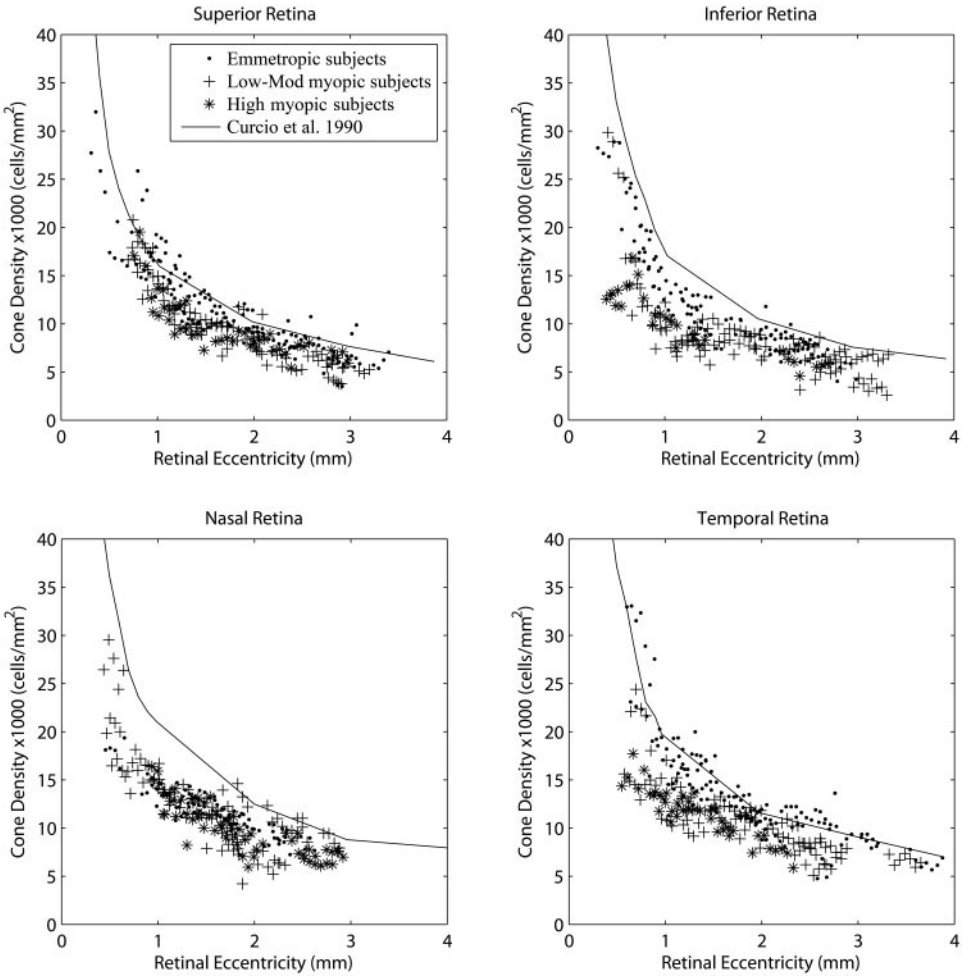

FIGURE 7. Comparison of cone packing density in the three groups of subjects differing in refractive error at four meridians. *Top right*: data for measurements along the superior meridian. *Filled symbols*: five subjects with emmetropia; *pluses*: four subjects with low-to-moderate myopia; *asterisks*: two subjects with high myopia. *Solid curve*: anatomic values based on published cone packing density in human retina from Curcio et al.[8] Other panels: comparison of cone packing density in the three groups of subjects along the inferior, nasal, and temporal meridians.

sults,[31–33] although perhaps with lower cell counts in the parafoveal retina, but it is not clear whether these represent individual differences or biases due to preparation. Curcio et al. presented the most detailed analysis of cone distributions. They found that cone packing density at 1 mm superior retina was ~16,000 cells/mm^2, corresponding to a cone spacing of 7.4 μm. Similarly, we found that cone packing density at 1 mm eccentricity in the superior retina was 15,121 cells/mm^2 in five emmetropic eyes, this corresponds to a cone spacing of 7.6 μm. In fact, we found considerable individual differences in cone packing density. Some subjects had cone packing density lower than those reported by Curcio et al. When we look at the results in our low-to-moderate and high myopic subjects, our data are much lower than the data of Curcio et al. However, the decrease in density with increasing retinal eccentricity is similar in all studies.

One of the goals of the present study was to provide a basis of comparison for studies of the effect of age and retinal pathology on cone packing density. This comparison requires careful optical modeling and determination of the exact positioning of the correction optics. For this reason, we also compared differences between eyes based on simple angular density of the cones—that is, using the visual angle rather than retinal size, which requires correcting the data for the axial length of the eye. As seen in Figure 9, the cone packing density was much more constant with axial length when expressed in

TABLE 1. Mean Cone Packing Densities Obtained from Two Retinal Areas in Four Meridians in Three Groups of Refractive Error

	Superior	Inferior	Nasal	Temporal	Average
Area 1 (0.9–1.0 mm)					
Emmetropic	16.868 ± 1.76	14.007 ± 2.03	13.994 ± 1.04	16.497 ± 3.17	15.341 ± 0.29
Low-moderate myopic	15.473 ± 1.64	9.891 ± 1.44	15.331 ± 0.93	13.681 ± 2.73	13.594 ± 0.32
High myopic	12.258 ± 1.20	10.837 ± 0.20	15.640 ± 0.91	12.864 ± 0.84	12.899 ± 0.43
Average	15.309 ± 2.44	11.773 ± 2.52	14.888 ± 1.16	14.991 ± 3.09	
Area 2 (1.8–2.0 mm)					
Emmetropic	9.942 ± 1.29	8.952 ± 0.38	10.212 ± 1.14	11.372 ± 1.06	10.119 ± 0.28
Low-moderate myopic	9.179 ± 1.52	8.201 ± 0.89	9.099 ± 3.11	10.887 ± 1.24	9.343 ± 2.56
High myopic	8.282 ± 0.81	6.759 ± 0.60	8.019 ± 1.33	8.626 ± 1.05	7.921 ± 0.44
Average	9.419 ± 1.41	8.211 ± 0.97	9.251 ± 2.22	10.963 ± 1.34	

Densities are expressed as ×1000 cells/mm^2 (mean ± SD).

TABLE 2. Main Effects and Interaction Effects of Refractive Group, Meridian, and Retinal Eccentricity on Cone Packing Density

Comparison by 3-Way ANOVA	*P*
Main effect of refractive group	<0.0001
Main effect of meridian	<0.0001
Main effect of retinal eccentricity	<0.0001
Interaction effect of refractive group × meridian	0.008
Interaction effect of refractive group × retinal eccentricity	0.228
Interaction effect of meridian × retinal eccentricity	0.007
Interaction among refractive group × meridian × retinal eccentricity	0.001

$P < 0.05$ was regarded as statistically significant.

cells per square degree of visual subtense than when expressed as cells pe square millimeter of retinal surface area (Fig. 8). This result means that, at least over this range of axial lengths, the data can be directly compared to a single set of subjects, without the need to measure and correct for axial length of the eye. Because in many hereditary retinal degenerations, eye size can be quite large, this result is reassuring. However, it is not known that the eye growth in hereditary retinal disease, or even in very high axial myopia, follows the same pattern.

The effect of eye growth can be explained by noting that the current data provide information on how differences in axial length, and presumably the subsequent retinal stretching and cone remodeling, varied at different retinal eccentricities and meridians. It is well established that the increase in the eye's axial length is greater than the increase in equatorial diameter as myopia develops,[17,34–36] but it is less clear whether the increase in axial length is distributed uniformly across the posterior pole or locally. One extreme example of a local growth would be if all the increase in axial length occurred as axial growth at the equator. We consider that it is unlikely that the cones are freely sliding across the entire surface of the retina during eye growth, since the vasculature is thought to constrain cone migration,[37,38] and because of this the cone packing density can be used to examine whether eye growth is causing local anisotropies or simply a uniform decrease in cone packing density. That is, a general expansion of the posterior pole should produce uniform changes in cone density, whereas a purely axial elongation at the equator should produce low cone densities at the equator, but normal everywhere else. Although we cannot measure cone density at the equator, our data do provide information on cone packing density within a few millimeters of the fovea. If the posterior pole grows uniformly, we would expect that between an eye with an axial length of 22 mm and one with an axial length of 28 mm, there would be a change of approximately 60% everywhere. This is not the case. At 1 mm in the superior retina, we found that the average cone packing density for an eye with an axial length of 28 mm was roughly 77% that of an eye with an axial length of 22 mm. Similarly, for data at 2 mm superior retina, the average cone packing density decreased to 75% with the same change in axial length. In contrast, for cone packing density at 1 mm nasal retina, the average cone packing density for an eye with an axial length of 28 mm was roughly 93% that of an eye with an axial length of 22 mm. For data at 2 mm nasal retina, a cone packing density decreased to approximately 79% with the same change in axial length. Therefore, our data are not consistent with a model of eye growth that occurs uniformly, with a consequent uniform decrease in cone packing density. Similarly, we can rule out the equatorial stretching model, which predicts similar cone packing densities in cells per square millimeter at the posterior pole for emmetropic and myopic eyes. Therefore, our data are also inconsistent with the hypothesis that the growth of the eye arises entirely from equatorial elongation. Thus, it is possible that that the elongation of the eye is differentially distributed across the posterior pole. This type of growth would still result in the well-established prolate shape with increased retinal surface area. However, the local increase in surface area would represent a complex combination of contributions. We cannot fully test this possibility, because of the limited range of retinal eccentricity tested in the present study, but there appeared to be local variations, with the smallest dependence on axial length occurring in the nasal retina. It is also important to note that this growth pattern may not be the same in extreme myopia or in hereditary retinal degeneration, but it suggests that a simple comparison of cone packing density based on the angular

TABLE 3. Multiple Comparisons of Cone Packing Densities for All Three Refractive Error Groups

Group		Difference	*P*
Emmetropic	Low-moderate myopic	1.673 ± 0.27	<0.001
	High myopic	2.313 ± 0.33	<0.001
Low-moderate myopic	High myopic	0.640 ± 0.35	0.156

The mean ± SD difference between emmetropic and the other two groups is significant, but the means of low-moderate myopic and high myopic are not significantly different. $P < 0.05$ was regarded as statistically significant.

TABLE 4. Regression Slopes for Cone Density in Four Meridians as a Function of Axial Length and Refractive Error

	Cone Density (cells/mm²) Regression Slope at Retinal Eccentricity			Cone Density (cells/deg²) Regression Slope at Retinal Eccentricity		
	1 mm	1.5 mm	2 mm	3 deg	5 deg	7 deg
Superior						
AL	−0.59*	−0.47*	−0.40*	0.04	0.02	0.02
Rx	0.32*	0.30*	0.27*	−0.02	−0.01	−0.003
Inferior						
AL	−1.41*	−0.88*	−0.62*	−0.04	−0.02	−0.003
Rx	0.73*	0.48*	0.34*	0.03	0.01	0.004
Nasal						
AL	−0.16	−0.30	−0.36	0.10*	0.05	0.03
Rx	0.06	0.14	0.18	−0.05*	−0.03	−0.02
Temporal						
AL	−1.38*	−0.51	−0.21	−0.06	0.03	0.05
Rx	0.71*	0.30	0.17	0.03	−0.01	−0.02

AL, axial length; Rx, refractive error.

* Regression slope was statistically significant at $P < 0.05$.

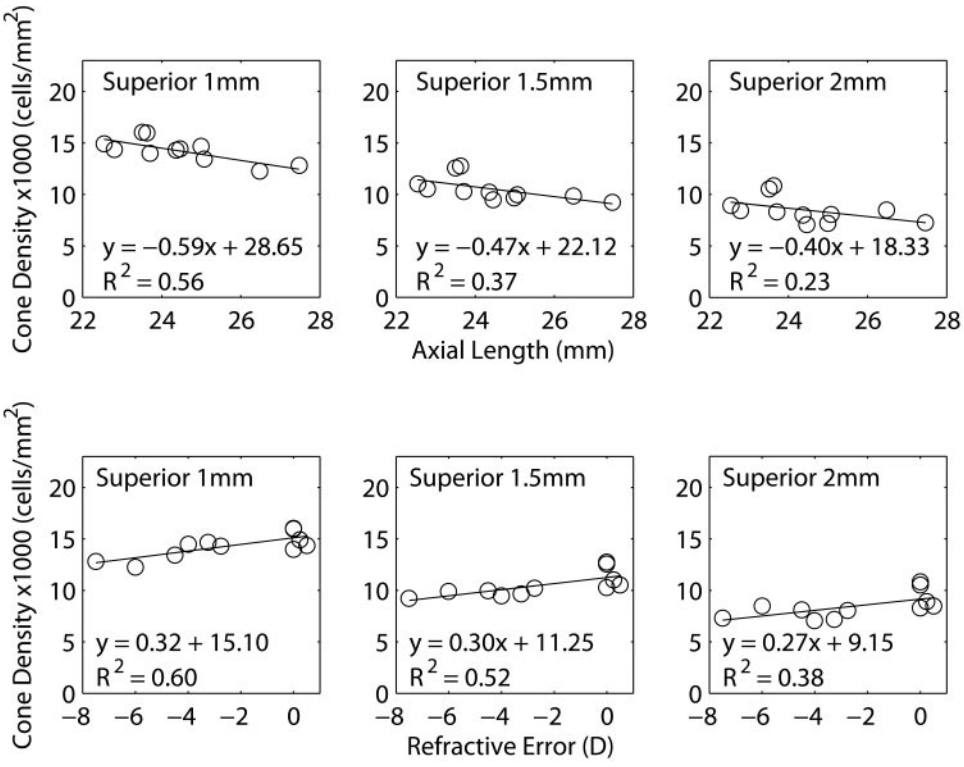

FIGURE 8. Variation of cone packing density with axial length (*top row*) and refractive error (*bottom row*) at three retinal eccentricities on the superior meridian. (○) Estimation of cone packing density in individual eyes; *solid line*: linear regression. All regression slopes are statistically significant ($P < 0.05$).

dimensions would be acceptable for determining normality of the cone mosaic.

These data are also related to studies that have examined the visual capabilities of persons with myopia. According to sampling theory, retinal resolution capability of the cone mosaic can be computed based on the spatial density of the retinal mosaic.[39] There is a large body of experimental evidence in support of this theory, with previous studies showing that retinal resolution acuity in cycles per millimeter is reduced with increasing myopia.[18–20,27] This result has been interpreted as evidence of retinal stretching of the myopic eye.[19–21,40] One possible explanation linking structure and function in myopic eyes is that retinal stretching caused by expansion of the posterior pole may lead to a reduction in neural sampling density.[19–21,40] That is, a

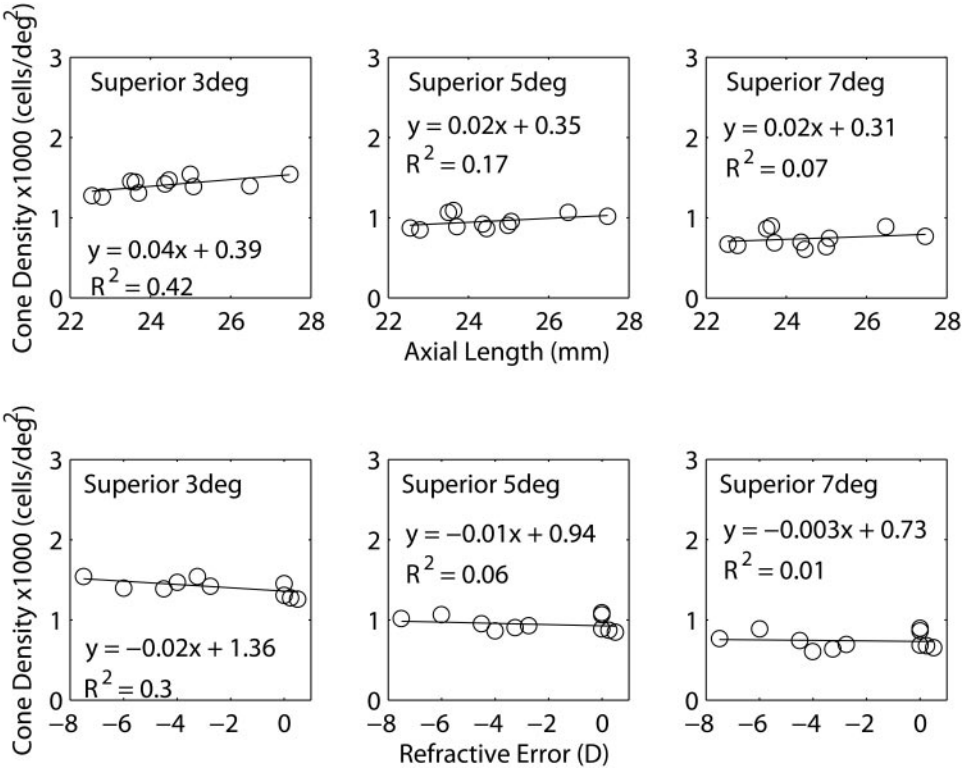

FIGURE 9. Variation of cone packing density with axial length (*top row*) and refractive error (*bottom row*) at three retinal eccentricities along the superior meridian. (○) Estimation of cone packing density from individual eyes; *solid line*: linear regression. All regression slopes are statistically nonsignificant ($P > 0.05$).

reduction in cone packing density has been interpreted as evidence of a visual acuity (cycles per millimeter) reduction in myopia that is most likely associated with retinal stretching in the myopic eye.[19–21,40] Our data allow us to compare actual cone measurements to data on acuity that have been published. Such a comparison is shown to the results of Coletta and Watson.[20] In this study an interferometer was used to investigate retinal resolution acuity at different retinal eccentricities as a function of refractive error.[20] Figure 10 shows, retinal resolution acuity measured at 4° and 10° retinal eccentricities in the temporal retina from the study of Coletta and Watson[20] compared with calculations based on the data from the present study. Because of the resolution limit of our system, we are not able to compare the foveal resolution acuity with this study. In the present study, the estimated cone packing densities at 4° and 10° retinal eccentricities were computed from the power law fits in 11 subjects. In approximating the actual cone packing arrangement within hexagonally packed samples,[41,42] the cone spacing (S) in micrometers is calculated as:

$$S = 1000[\sqrt{3}/(2D)]^{1/2}, \quad (1)$$

where S is defined as the center-to-center spacing of cones in micrometers, and D is the cone density in cells per square millimeter. The Nyquist limit of resolution (*Vn*) in cycles per millimeter is then calculated as:

$$Vn = [\sqrt{3}(S/1000)]^{-1}, \quad (2)$$

where S, in micrometers, is obtained from equation 1. The results of these calculations for our study at 4° and 10° retinal eccentricities in the temporal retinal appear in Figure 10 as the filled and open circles, respectively. The solid lines in Figure 10, are results of linear regressions for 4° and 10° retinal eccentricities from the study of Coletta and Watson.[20] The dashed lines are the linear regressions to the predicted retinal resolution acuity from the present study. Coletta and Watson reported that the retinal resolution acuity at 4° temporal retina was 79 cyc/mm in an emmetropic eye. In contrast, our data indicate that the predicted retinal resolution acuity at 4° temporal retina should be 77 cyc/mm in an emmetropic eye. According to the regression slopes in Figure 10, the reduction in the rate of retinal resolution acuity with refractive error at retinal eccentricity of 4° are 1.34 and 2.00 cyc/mm per diopter in the study by Coletta and Watson[20] and the present study, respectively. Thus, our data show a steeper decline in cone packing density then would be inferred from their data, but the difference is small. Looking at the data for 10°, there is an offset between their measurements and our prediction, probably based on the well-documented finding that retinal resolution acuity is limited by the P-type retinal ganglion cell density not cone packing density beyond 10° to 15° retinal eccentricity.[43–45] Here, however, we found that the variation with refractive error was similar. Thus, both data sets indicate that myopic eyes have lower retinal resolution acuity than do emmetropic eyes. Therefore, our study provides further evidence in support of the hypothesis that retinal stretching in myopic eyes reduces retinal sampling density.

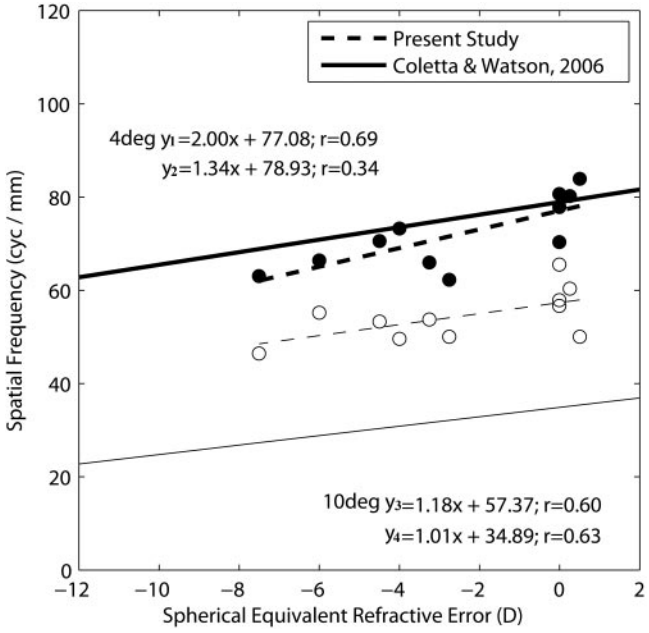

FIGURE 10. Relationship between retinal resolution acuity and spherical equivalent refractive error. *y*-Axis: retinal resolution acuity. Data are the computed temporal retinal resolution acuity at (●) 4° and (○) 10° retinal eccentricities. *Dashed lines*: linear fits to the data at 4° (y_1: *heavy dashed line*) and 10° (y_3: *light dashed line*). *Solid lines*: the linear regression of retinal resolution acuity at 4° (y_2: *heavy solid line*) and 10° (y_4: *light solid line*) from Coletta and Watson.[20]

CONCLUSIONS

In summary, our results provide a baseline analysis of cone packing density in vivo in relatively young, healthy human eyes. The baseline data are useful for detecting and monitoring the loss of cone photoreceptors in retinal diseases. This study has also demonstrated that in terms of cones per square millimeter, there is a systematic decrease in cone packing density with increasing axial length. Thus, as predicted by retinal stretching, cone packing density is lower in highly myopic eyes than in emmetropic eyes. Our emmetropic eyes had cone packing density similar to that reported by Curcio et al.[8] but our myopic eyes had lower packing densities. We found a similar variation in cone packing density with changes in retinal eccentricity and meridian to those reported by Curcio et al. with the exception of the nasal meridian, where we found somewhat lower cone packing densities. Although our data do not have sufficient power to test differences between different degrees of refractive error, they suggest that such changes would be present, as expected from the need to distribute a constant number of cones over a larger retinal surface area.

Acknowledgments

The authors thank Arthur Bradley for helpful discussions.

References

1. Liang J, Williams DR, Miller DT. Supernormal vision and high-resolution retinal imaging through adaptive optics. *J Opt Soc Am A Opt Image Sci Vis*. 1997;14:2884–2892.
2. Roorda A, Romero-Borja F, Donnelly WJ, Queener H, Hebert TJ, Campbell MCW. Adaptive optics scanning laser ophthalmoscopy. *Opt Express*. 2002;10:405–412.
3. Roorda A. Adaptive optics ophthalmoscopy. *J Refract Surg*. 2000; 16:S602–S607.
4. Pircher M, Zawadzki RJ, Evans JW, Werner JS, Hitzenberger CK. Simultaneous imaging of human cone mosaic with adaptive optics enhanced scanning laser ophthalmoscopy and high-speed transversal scanning optical coherence tomography. *Opt Lett*. 2008;33:22–24.
5. Duncan JL, Zhang Y, Gandhi J, et al. High-resolution imaging with adaptive optics in patients with inherited retinal degeneration. *Invest Ophthalmol Vis Sci*. 2007;48:3283–3291.

6. Wolfing JI, Chung M, Carroll J, Roorda A, Williams DR. High-resolution retinal imaging of cone-rod dystrophy. *Ophthalmology*. 2006;113:1014–1019.
7. Carroll J, Neitz M, Hofer H, Neitz J, Williams DR. Functional photoreceptor loss revealed with adaptive optics: an alternate cause of color blindness. *Proc Natl Acad Sci U S A*. 2004;101:8461–8466.
8. Curcio CA, Sloan KR, Kalina RE, Hendrickson AE. Human photoreceptor topography. *J Comp Neurol*. 1990;292:497–523.
9. Marcos S, Burns SA. Cone spacing and waveguide properties from cone directionality measurements. *J Opt Soc Am A Opt Image Sci Vis*. 1999;16:995–1004.
10. Williams DR. Topography of the foveal cone mosaic in the living human eye. *Vision Res*. 1988;28:433–454.
11. Curcio CA, Owsley C, Jackson GR. Spare the rods, save the cones in aging and age-related maculopathy. *Invest Ophthalmol Vis Sci*. 2000;41:2015–2018.
12. Jackson GR, Owsley C, Curcio CA. Photoreceptor degeneration and dysfunction in aging and age-related maculopathy. *Ageing Res Rev*. 2002;1:381–396.
13. Bullimore MA, Gilmartin B, Royston JM. Steady-state accommodation and ocular biometry in late-onset myopia. *Doc Ophthalmol*. 1992;80:143–155.
14. McBrien NA, Millodot M. A biometric investigation of late onset myopic eyes. *Acta Ophthalmol*. 1987;65:461–468.
15. Grosvenor T, Scott R. Three-year changes in refraction and its components in youth-onset and early adult-onset myopia. *Optom Vis Sci*. 1993;70:677–683.
16. Grosvenor T, Scott R. Role of the axial length/corneal radius ratio in determining the refractive state of the eye. *Optom Vis Sci*. 1994;71:573–579.
17. Atchison DA, Jones CE, Schmid KL, et al. Eye shape in emmetropia and myopia. *Invest Ophthalmol Vis Sci*. 2004;45:3380–3386.
18. Atchison DA, Schmid KL, Pritchard N. Neural and optical limits to visual performance in myopia. *Vision Res*. 2006;46:3707–3722.
19. Chui TY, Yap MK, Chan HH, Thibos LN. Retinal stretching limits peripheral visual acuity in myopia. *Vision Res*. 2005;45:593–605.
20. Coletta NJ, Watson T. Effect of myopia on visual acuity measured with laser interference fringes. *Vision Res*. 2006;46:636–651.
21. Strang NC, Winn B, Bradley A. The role of neural and optical factors in limiting visual resolution in myopia. *Vision Res*. 1998;38:1713–1721.
22. Kitaguchi Y, Bessho K, Yamaguchi T, Nakazawa N, Mihashi T, Fujikado T. In vivo measurements of cone photoreceptor spacing in myopic eyes from images obtained by an adaptive optics fundus camera. *Jpn J Ophthalmol*. 2007;51:456–461.
23. Collins JW, Carney LG. Visual performance in high myopia. *Curr Eye Res*. 1990;9:217–223.
24. Subbaram MV, Bullimore MA. Visual acuity and the accuracy of the accommodative response. *Ophthalmic Physiol Opt*. 2002;22:312–318.
25. Fiorentini A, Maffei L. Spatial contrast sensitivity of myopic subjects. *Vision Res*. 1976;16:437–438.
26. Jaworski A, Gentle A, Zele AJ, Vingrys AJ, McBrien NA. Altered visual sensitivity in axial high myopia: a local postreceptoral phenomenon? *Invest Ophthalmol Vis Sci*. 2006;47:3695–3702.
27. Rossi EA, Weiser P, Tarrant J, Roorda A. Visual performance in emmetropia and low myopia after correction of high-order aberrations. *J Vis*. 2007;7:14.
28. Paquin MP, Hamam H, Simonet P. Objective measurement of optical aberrations in myopic eyes. *Optom Vis Sci*. 2002;79:285–291.
29. Salmon TO, West RW, Gasser W, Kenmore T. Measurement of refractive errors in young myopes using the COAS Shack-Hartmann aberrometer. *Optom Vis Sci*. 2003;80:6–14.
30. Burns SA, Tumbar R, Elsner AE, Ferguson D, Hammer DX. Large-field-of-view, modular, stabilized, adaptive-optics-based scanning laser ophthalmoscope. *J Opt Soc Am A Opt Image Sci Vis*. 2007;24:1313–1326.
31. Jonas JB, Schneider U, Naumann GO. Count and density of human retinal photoreceptors. *Graefes Arch Clin Exp Ophthalmol*. 1992;230:505–510.
32. Sjostrand J, Conradi N, Klaren L. How many ganglion cells are there to a foveal cone? A stereologic analysis of the quantitative relationship between cone and ganglion cells in one normal human fovea. *Graefes Arch Clin Exp Ophthalmol*. 1994;232:432–437.
33. Sjostrand J, Olsson V, Popovic Z, Conradi N. Quantitative estimations of foveal and extra-foveal retinal circuitry in humans. *Vision Res*. 1999;39:2987–2998.
34. Meyer-Schwickerath G, Gerke E. Biometric studies of the eyeball and retinal detachment. *Br J Ophthalmol*. 1984;68:29–31.
35. Curtin BJ, Karlin DB. Axial length measurements and fundus changes of the myopic eye. *Am J Ophthalmol*. 1971;1:42–53.
36. Logan NS, Gilmartin B, Wildsoet CF, Dunne MC. Posterior retinal contour in adult human anisomyopia. *Invest Ophthalmol Vis Sci*. 2004;45:2152–2162.
37. Springer AD, Hendrickson AE. Development of the primate area of high acuity, 3: temporal relationships between pit formation, retinal elongation and cone packing. *Vis Neurosci*. 2005;22:171–185.
38. Springer AD, Hendrickson AE. Development of the primate area of high acuity. 1. Use of finite element analysis models to identify mechanical variables affecting pit formation. *Vis Neurosci.* 2004;21:53–62.
39. Helmholtz HV. Treatise on physiological optics. *Opt Soc Am.* 1924;2:1–46.
40. Bradley A, Rabin J, Freeman RD. Nonoptical determinants of aniseikonia. *Invest Ophthalmol Vis Sci*. 1983;24:507–512.
41. Snyder AW, Miller WH. Photoreceptor diameter and spacing for highest resolving power. *J Opt Soc Am*. 1977;67:696–698.
42. Hirsch J, Miller WH. Does cone positional disorder limit resolution? *J Opt Soc Am A*. 1987;4:1481–1492.
43. Anderson RS, Wilkinson MO, Thibos LN. Psychophysical localization of the human visual streak. *Optom Vis Sci*. 1992;69:171–174.
44. Anderson SJ, Mullen KT, Hess RF. Human peripheral spatial resolution for achromatic and chromatic stimuli: limits imposed by optical and retinal factors. *J Physiol*. 1991;442:47–64.
45. Thibos LN, Cheney FE, Walsh DJ. Retinal limits to the detection and resolution of gratings. *J Opt Soc Am* [*A*]. 1987;4:1524–1529.